Voltage Support Provided by a Droop-Controlled Multifunctional Inverter

Juan C. Vasquez, R. A. Mastromauro, *Member, IEEE*, Josep M. Guerrero, *Senior Member, IEEE*, and Marco Liserre, *Senior Member, IEEE*

***Abstract*—This paper presents a single-phase multifunctional inverter for photovoltaic (PV) systems application. The converter provides active power to local loads and injects reactive power into the grid providing voltage support at fundamental frequency. The proposed topology is controlled by means of the droop-control technique. Hence, it allows the obtaining of voltage-sag-compensation capability, endowing voltage ride-through to the system. A model and analysis of the whole system is given to properly choose the control parameters. Simulation and experimental results validate the proposed control using a 5-kVA PV converter.**

***Index Terms*—Droop-control technique, single-phase photovoltaic (PV) inverter, voltage ride-through, voltage-source inverter (VSI).**

I. Introduction

The IEEE Standard 1547 [1], [2] defines the ancillary services in distributed power generation systems (DPGSs) as follows: load regulation, energy losses, spinning and nonspinning reserves, voltage regulation, and reactive-power supply. It recommends that low-power systems should be disconnected when the grid voltage is lower than 0.85 p.u. or higher than 1.1 p.u., as an anti-islanding requirement [1], [2]. Among low-power DPGS, the number of photovoltaic (PV) plants connected to low-voltage distribution lines has been increasing in the later years [3], [4]. Hence, the distributed PV systems should be designed to comply with anti-islanding requirements, but they can also sustain the voltage for local loads.

Usually, grid-connected PV inverters work like current sources, in which the voltage reference is often taken from the grid-voltage sensing using a phase-locked-loop circuit, while an inner current loop ensures that the inverter acts as a current source. However, in order to maintain the voltage and frequency stabilities, voltage-source inverters (VSIs) are convenient, since they can provide to the DPGS performances like ride-through capability, island-mode operation, power-quality enhancement, and microgrid functionalities [5].

Several control techniques based on the droop method have been proposed to connect VSI system in parallel to avoid communications between them. Droop method can be an interesting way to control active and reactive powers injected to the grid. However, in this last case, the droop method has several problems to be solved, like line-impedance dependence, bad regulation of active and reactive powers, and slow transient response.

This paper is focused on a grid-connected PV system improved with additional power-quality conditioning functionalities. The PV grid-connected converter is controlled on the basis of the droop-control technique [5]–[8] which provides the voltage reference for the repetitive controller [9], [10]. The proposed system can support the voltage applied to local loads also in the presence of voltage sags.

This paper is organized as follows. In Section II, the possible voltage and frequency support provided by a DPGS converter connected to the grid is discussed. A single-phase PV system improved with voltage-sag-mitigation functionality is proposed in Section III. In Section IV, the control objectives and the control design are presented. Section V shows the analysis of the system dynamics to perform the design of the control parameters. Simulation and experimental results are presented in Sections VI and VII, respectively, in order to validate the proposed control strategy. Finally, in Section VIII, the conclusions are given.

II. Voltage and Frequency Support

The power transfer between two sections of the line connecting a DPGS converter to the grid can be derived using the infinite bus model and complex phasors. The analysis as follows is valid for both single-phase and balanced three-phase systems. As shown in Fig. 1, when the DPGS inverter is connected to the grid through a generic impedance, the active and reactive powers injected to the grid can be expressed as follows:

$$P = \frac{1}{Z}\left[(EV\cos\phi - V^2)\cos\theta + EV\sin\phi\sin\theta\right] \quad (1)$$

$$Q = \frac{1}{Z}\left[(EV\cos\phi - V^2)\sin\theta - EV\sin\phi\cos\theta\right] \quad (2)$$

where E is the VSI voltage, V is the grid voltage, and ϕ is the phase between E and V. Considering that the line impedance is mainly inductive $X \gg R$, R may be neglected. Consequently, (1) and (2) can be rewritten as

$$P = \frac{EV}{X}\sin\phi \quad (3)$$

$$Q = \frac{EV\cos\phi - V^2}{X}. \quad (4)$$

Manuscript received November 3, 2008; revised January 29, 2009. First published February 24, 2009; current version published October 9, 2009.

J. C. Vasquez and J. M. Guerrero are with the Department of Automatic Control Systems and Computer Engineering, Technical University of Catalonia, 08036 Barcelona, Spain (e-mail: juan.carlos.vasquez@upc.edu; josep.m.guerrero@upc.edu).

R. A. Mastromauro and M. Liserre are with the Department of Electrical and Electronic Engineering, Politecnico di Bari, 70125 Bari, Italy.

Color versions of one or more of the figures in this paper are available online at http://ieeexplore.ieee.org.

Digital Object Identifier 10.1109/TIE.2009.2015357

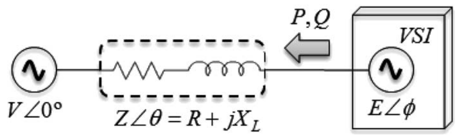

Fig. 1. Power flow through a line.

Arranging (3) and (4) and considering that the power angle ϕ is small, then $\sin\phi \cong \phi$ and $\cos\phi \cong 1$; the phase and the voltage difference between the grid and the VSI can be calculated as

$$\phi \approx \frac{X}{EV}P \tag{5}$$

$$E - V \approx \frac{X}{V}Q. \tag{6}$$

From these equations, it is possible to deduce that the power angle depends predominantly on the active power, whereas the voltage difference $E - V$ depends predominantly on the reactive power. In other words, the angle ϕ can be controlled by regulating the active power, whereas the inverter voltage E is controllable through the reactive power. The frequency control dynamically controls the power angle and, hence, the real power flow. Thus, by adjusting the active power P and the reactive power Q independently, frequency and amplitude of the grid voltage are determined. These conclusions form the basis of the frequency and voltage droop control through, respectively, active and reactive powers.

III. Multifunctional Converter for Voltage-Sag Mitigation

A. Shunt Converter for Voltage-Sag Mitigation

Often, series-converter topologies using instantaneous power theory are applied to multifunctional inverters with ride-through capability in the presence of grid-voltage sags [19], [20]. Alternatively, shunt devices are usually adopted to compensate for small voltage variations which can be controlled by reactive-power injection. Examples of applications can be found in line-interactive uninterruptible power systems or active-power filter topologies [11]–[17]. The ability to control the fundamental voltage at a certain point depends on the grid impedance and the power factor of the load. The compensation of voltage sags by current injection is difficult to achieve, because the grid impedance is usually low and the injected current has to be very high to increase the load voltage. The shunt converter can be current or voltage controlled as shown in Fig. 2. Following these diagrams in the figure, it is possible to observe that

$$\vec{I_C} = \vec{I}_G + \vec{I}_L \tag{7}$$

where I_C, I_G, and I_L are the currents delivered from the converter, to the grid, and to the load, respectively. Fig. 3(a) shows the vector diagram of the voltage and currents.

Note that when the amplitudes E and V are equal, only active power (direct I_G) flows into the inductor L_G. Therefore, if the

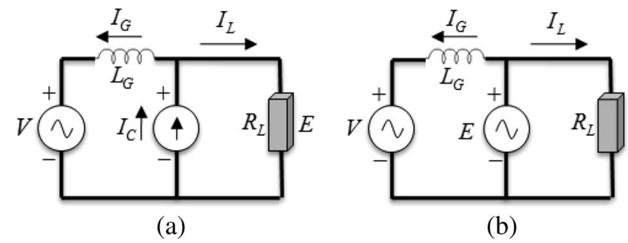

Fig. 2. Equivalent circuit of the power stage of shunt converters for voltage-sag compensation. (a) Current-controlled and (b) voltage-controlled shunt converter.

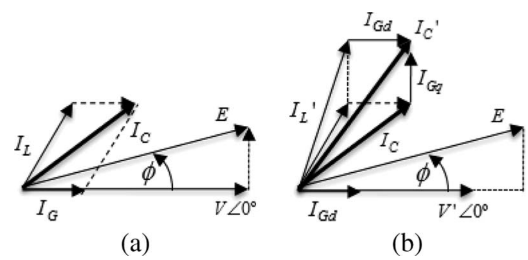

Fig. 3. Vector diagram of the shunt converter providing both active and reactive powers. (a) Normal conditions. (b) Vector diagram for compensation of a voltage sag of 0.15 p.u.

controller is designed to provide only reactive power, when a voltage sag occurs $V' < E$, and

$$\vec{I'_G} = I_{Gd} + jI_{Gq} \tag{8}$$

with $I_{Gd} = I_G$, and $\vec{I}_{Gq}$ is the reactive current needed to compensate the voltage sag. The amplitude of the grid current depends on the value of the grid impedance since

$$\vec{I_G} = \frac{E\angle\phi - V\angle 0^\circ}{jX} \tag{9}$$

where X is the inductor reactance (ωL_G). If the shunt controller supplies the load with both active and reactive powers, in normal conditions, it provides a compensating current $\vec{I}_C = \vec{I}_L$; hence, the system operates as in island mode, and $\vec{I}_G = 0$. In the case of a voltage sag, the converter has to provide the active power required by the load and must still inject the reactive power needed to stabilize the load voltage as shown in Fig. 3(b). The grid current in this case is mainly reactive. It can be observed that during a voltage sag, the amount of reactive current needed to maintain the load voltage at the desired value is inversely proportional to the grid impedance. This means that a large inductance will help in mitigating voltage sags.

B. Power-Stage Configuration

In case of PV systems, it can be advantageous to use the shunt-connected PV converter also for the compensation of small voltage sags. In this hypothesis, it is possible to control the voltage directly in order to stabilize the voltage profile while the current injection is controlled indirectly. Hence, the converter acts as a voltage source, supplying the load and maintaining constant the load voltage. Usually, the impedance of low-voltage distribution lines is mainly resistive, but in the

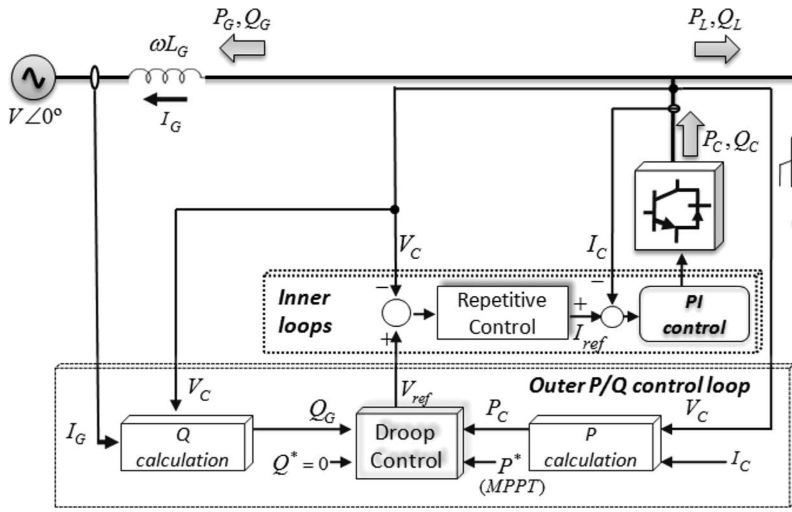

Fig. 4. Block diagram of the grid-connected PV-system power stage and its control scheme.

proposed topology, the PV converter is parallel connected to the grid through an extra inductance L_G (as shown in Fig. 2).

From the exact expression of (3), we can conclude that the maximum active power transferred from or to the grid limits the maximum value of the inductance, as follows:

$$X < \frac{EV}{P_{\max}} \tag{10}$$

whereas $P_{\max}$ is the maximum active power delivered by the VSI ($\phi = 90°$). By adding this inductance (L_G), the grid can be considered mainly inductive. In this hypothesis, it is possible to control the frequency and the voltage amplitude by adjusting active and reactive powers independently. However, it is not convenient to choose a high-value inductance L_G, since the voltage regulation is directly affected by its voltage drop.

The PV system shown in Fig. 4 is controlled in order to provide the active and reactive powers required. The converter is controlled with three control loops: In the outer one, the droop controller provides the voltage reference for the repetitive controller based on the relationship of Fig. 5. It is possible to modify this voltage reference with the addition of another control loop designed to eliminate the average current present in the system due to a small offset in the inverter output voltage. This offset can be generated by errors in the voltage and current sensors and by the physical differences between the upper and lower switches of the legs in the PWM inverter bridge [19], [20]. The new reference voltage is shown in Fig. 4 as V_{ref}. Hence, the voltage error is preprocessed by the repetitive controller which is the periodic signal generator of the fundamental component and of the selected harmonics. This kind of controller is suitable in case of using nonlinear loads, since it is able to supply current harmonics while maintaining low-voltage THD. In this case, the third and the fifth ones are compensated [9], [10]. Finally, the *PI* controller, in the inner loop, improves the stability of the system offering low-pass filter function. In the presence of a voltage sag, the grid current I_G is forced by the controller to have a sinusoidal waveform which is phase shifted by almost 90° with respect to the corresponding grid voltage (Figs. 6 and 7).

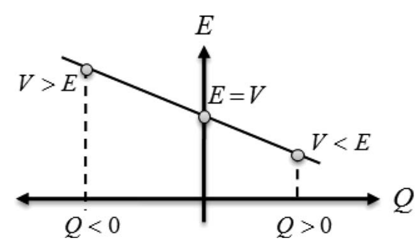

Fig. 5. Relationship between the droop-based controller.

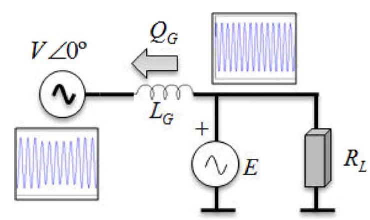

Fig. 6. Power-flow circuit in the presence of a voltage dip.

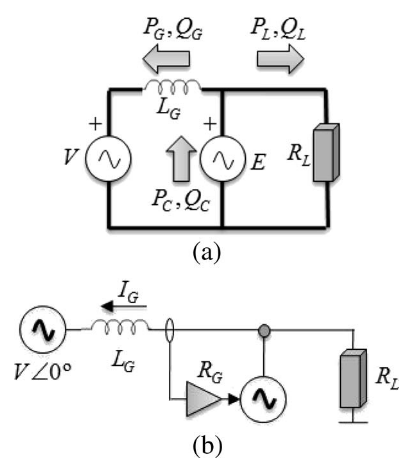

Fig. 7. Power-flow-based circuit modeling. (a) Equivalent circuit. (b) General approach.

IV. Control Design

The aim of this section is to develop a control structure for the proposed PV shunt-connected converter. The control objectives of the droop-based controller can be summed up as follows:

1) enhances the stability and the dynamic response by damping the system;
2) provides all the active power given by the PV source and extracted in the previous stage by the maximum-power point tracker (MPPT) [18];
3) supports the reactive power required by the grid when voltage sag is presented into the grid [21].

These three control objectives can be achieved by using the following control loops: The first one is done by implementing a virtual resistor, via the VSI control [5]

$$V_{ref} = V^*_{ref} - I_G \cdot R_G. \tag{11}$$

However, adding damping into the system implies that the impedance seen by the VSI is not purely inductive, i.e., $R_G + j\omega L_G$.

Fig. 4 shows the block diagram of this proposed control strategy in which V_C and I_C denote the converter voltage and current, respectively, and I_G is the grid current. By multiplying V_C by I_C and filtering the result, it is possible to obtain the active power delivered by the converter (P_C). On the other hand, multiplying V_C delayed 90° by I_G, and then filtering the resulting value, the reactive power flow from/to the grid (Q_G) can be obtained

$$P_C \cong \frac{1}{Z}\left[V(E-V)\cos\theta + EV\cdot\phi\cdot\sin\theta\right] \tag{12}$$

$$Q_G \cong \frac{1}{Z}\left[(V(E-V)\sin\theta - EV\cdot\phi\cdot\cos\theta\right] \tag{13}$$

where $\theta = X/R$. Based on the information shown in Fig. 1, it is possible to calculate both the active P and reactive Q powers injected to the grid by the VSI, as shown in (1) and (2). For possible simplifications, it is possible to transform P and Q to novel variables defined as P' and Q', which are independent from the magnitude and phase of the grid impedance

$$P' = P_C\sin\theta - Q_G\cos\theta \tag{14}$$

$$Q' = P_C\cos\theta + Q_G\sin\theta. \tag{15}$$

By substituting (12) and (13) into (14) and (15), the following expressions are yielded:

$$P' = \frac{EV}{Z}\sin\phi \tag{16}$$

$$Q' = \frac{EV}{Z}\cos\phi - V^2. \tag{17}$$

Note that P' is mainly dependent on the phase ϕ, while Q' depends on the voltage difference between the VSI and the grid $(E - V)$, as in purely inductive case (5) and (6).

These new control variables (P' and Q') are independent from the grid-impedance angle θ, thus we can use them into the droop method to control the active and reactive power flows. In order to inject the desired active power (P^*_C, which should coincide with the power given by the MPPT) and to compensate the reactive power (normally $Q^*_C = 0$), the following droop-method control loops which uses the transformation (14) and (15) are proposed:

$$\phi = -G_p(s)\left[(P_C - P^*_C)\sin\theta - (Q_G - Q^*_G)\cos\theta\right] \tag{18}$$

$$E = E^* - G_q(s)\left[(P_C - P^*_C)\cos\theta + (Q_G - Q^*_G)\sin\theta\right]. \tag{19}$$

A *PI* controller is proposed to ensure that the VSI injects the active power delivered by the MPPT stage. On the other hand, a proportional controller is proposed for the reactive-power compensation defined as $G_p(s)$ and $G_q(s)$, respectively,

$$G_p(s) = \frac{m_i + m_p s}{s} \tag{20}$$

$$G_q(s) = n_p. \tag{21}$$

For reactive-power compensation support, the coefficient n_p must be properly adjusted. By using (4), (6), (19), and (21) with $\theta \cong 90°$ and $V = \alpha E^*$ (where α is the voltage-sag percentage), it is possible to obtain

$$n_p = \frac{E^*\alpha(1-\alpha) - Q_{\max}X}{Q_{\max}E^*\alpha} \tag{22}$$

where $Q_{\max}$ is the maximum reactive-power flow that can be delivered by the VSI. Fig. 8 shows details of the block-diagram implementation of the droop controller, which is able to inject the desired active power P^*_C and to compensate reactive power Q_G.

V. System Dynamics and Control-Design Parameters

In this section, the system-dynamic model and the stability analysis are provided to properly design m_i and m_p coefficients of the *PI* compensator (20), corresponding to the active-power-injection control loop (18).

A small-signal analysis is provided in order to show the system stability and the transient response. The power-calculation block uses a low-pass second-order filter in which the passband is much smaller than the passband of the inverter-voltage control. Hence, both the power and reactive output power measured from the power-calculation block can be defined as

$$\hat{p}_{\text{meas}}(s) = \frac{\omega_o^2}{s^2 + 2\zeta\omega_o s + \omega_o^2}\cdot\hat{p}'(s) \tag{23}$$

$$\hat{q}_{\text{meas}}(s) = \frac{\omega_o^2}{s^2 + 2\zeta\omega_o s + \omega_o^2}\cdot\hat{q}'(s) \tag{24}$$

where ω_o is the resonance frequency and ζ the damped coefficient. By doing a small-signal approximation in order to linearize the equations, it yields

$$\hat{p}_{\text{meas}}(s) = \frac{\omega_o^2}{s^2 + 2\zeta\omega_o s + \omega_o^2}\left[\frac{V\sin\Phi\hat{e}(s) + VE\cos\Phi\hat{\phi}(s)}{Z}\right] \tag{25}$$

$$\hat{q}_{\text{meas}}(s) = \frac{\omega_o^2}{s^2 + 2\zeta\omega_o s + \omega_o^2}\left[\frac{V\cos\Phi\hat{e}(s) - VE\sin\Phi\hat{\phi}(s)}{Z}\right] \tag{26}$$

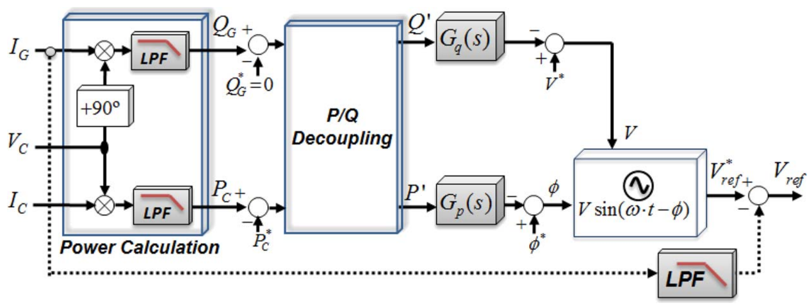

Fig. 8. Block diagram of the droop-control loops.

where the lower case variables with the symbol ^ indicate small-signal values and uppercase variables are the steady-state values. By using (20) and (21), (24), and (25), we can obtain

$$\hat{\phi}(s) = -\frac{m_i + m_p s}{s}\hat{p}_{\mathrm{meas}}(s) \tag{27}$$

$$\hat{e}(s) = -n_i \hat{q}_{\mathrm{meas}}(s). \tag{28}$$

From (26) and (27), the following expressions can be derived:

$$\hat{\phi}(s) = -\frac{m_i + m_p s}{s}\cdot\left(V\sin\Phi\hat{e}(s) + VE\cos\Phi\hat{\phi}(s)\right) \tag{29}$$

$$\hat{e}(s) = -n_i\cdot\left(V\cos\Phi\hat{e}(s) - VE\sin\Phi\hat{\phi}(s)\right). \tag{30}$$

By combining (28) and (29), we can be obtain the following fifth-order characteristic equation:

$$s^5 + a_4 s^4 + a_3 s^3 + a_2 s^2 + a_1 s + a_0 = 0. \tag{31}$$

Being

$$\begin{aligned}
a_4 &= 4\omega_o\zeta Z \\
a_3 &= V\omega_o^2\cos\Phi(n_p + Em_p) + 2\omega_o^2(1+2\zeta^2)Z \\
a_2 &= 2V\omega_o^2\zeta\cos\Phi(n_p + Em_p) + \omega_o^2 VE\cos\Phi m_i + 4\zeta\omega_o^3 Z \\
a_1 &= V\omega_o^4\cos\Phi(n_p + Em_p) \\
&\quad + VE\omega_o^3\left(2\zeta\cos\Phi m_i + \frac{V}{Z}\omega_o n_p m_p\right) + \omega_o^4 Z \\
a_0 &= VE\omega_o^4 m_i\left(\cos\Phi + \frac{V}{Z}n_p\right)
\end{aligned}$$

the steady-state values of the active power are $P = P^*$, and calculating Q using (2) in steady state, defined as

$$Q_{ss} = \frac{1}{Z}\left[(EV\cos\Phi - V^2)\sin\theta - EV\sin\Phi\cos\theta\right] \tag{32}$$

the steady-state phase and amplitudes can be calculated from (12) and (13), as follows:

$$\Phi = \tan^{-1}\left(\frac{P_C^*\sin\theta - Q_{SS}\cos\theta}{P_C^*\cos\theta + Q_{ss}\cdot\sin\theta + (V^2/Z)}\right) \tag{33}$$

$$E = \frac{V^2\cos\theta + P_C^* Z}{V(\cos\theta\cos\Phi + \sin\theta\sin\Phi)}. \tag{34}$$

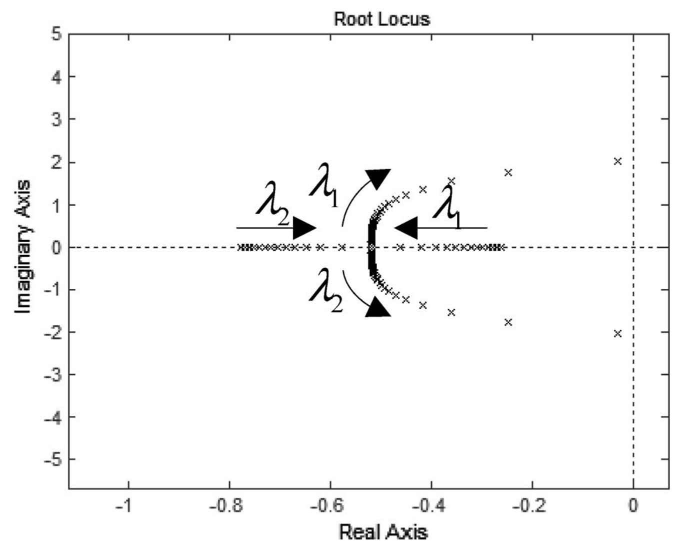

Fig. 9. Root locus for $0.00002 < m_p < 0.001$ and $m_i = 0.0002$.

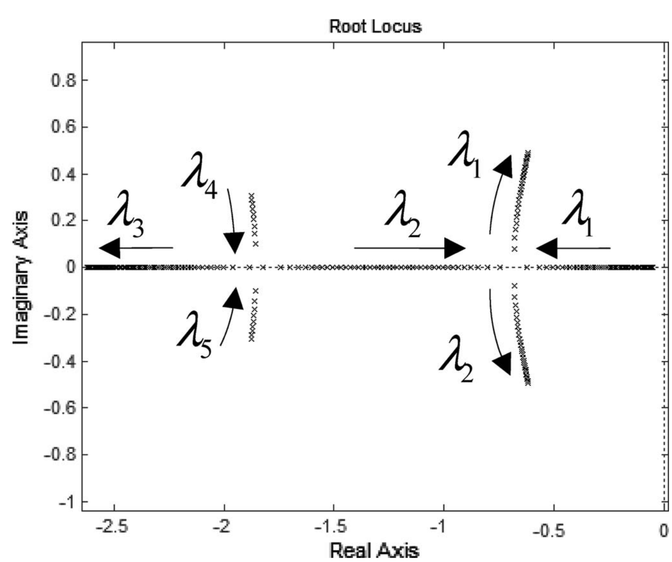

Fig. 10. Root locus for $0.000002 < m_i < 0.0018$ and $m_p = 0.00006$.

The model obtained has been used to extract the family of root locus as shown in Figs. 9 and 10. Fig. 9 shows, for convenience, the dominant poles (λ_1 and λ_2) root locus. It illustrates that, when m_p is increased, the poles go toward the imaginary axis, becoming a faster oscillatory system. Fig. 10 shows the root-locus behavior when m_i is increased. Note that λ_3, λ_4, and λ_5 are far away from λ_1 and λ_2. Thus, using m_p and m_i,

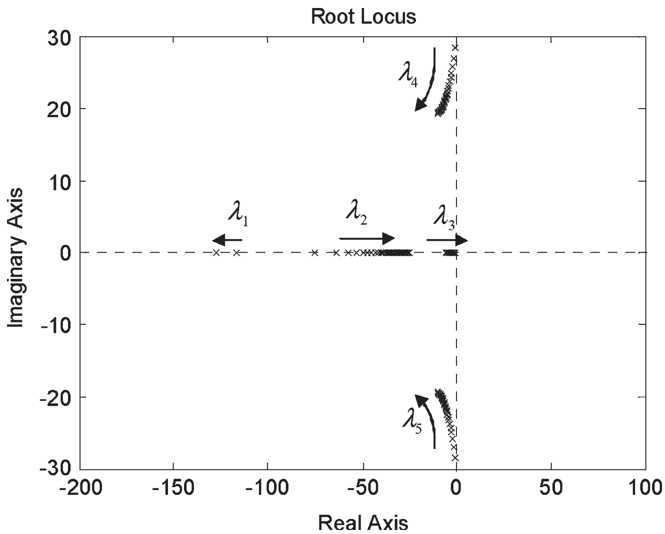

Fig. 11. Root-locus diagram for grid-inductance variations: 8.5 mH $< L_G <$ 5000 mH.

TABLE I
POWER-STAGE AND CONTROL PARAMETERS

Symbol	*Parameter*	*Value*	*Unit*
E	Grid voltage amplitude	311	V
ω^*	Grid frequency	2π50	rd/s
R	Load resistance	40	Ω
L_G	Grid inductance	15	mH
fs	Sampling frequency	6400	Hz
m_i	Integral droop P' coefficient	0.00002	W s/rd
m_p	Proportional droop P' coefficient	0.0002	W/rd
n_p	Proportional droop Q' coefficient	0.006	VArs s/V
ω_o	Resonance frequency of measuring filter	31.4	rd/s

it is possible to locate the poles where it is more convenient. Furthermore, this dominance can illustrate that the obtained model can be adjusted as a second- or even a first-order system.

By using this model (31), the stability of the system has been studied for large grid-inductance L_G variations. Fig. 11 shows that the fifth-order system is stable if the value of L_G is more than 8 mH. Below this value, the real part of the eigenvalues λ_4 and λ_5 is positive, so the system remains unstable. On the contrary, if we increase the value of L_G, those eigenvalues are stable. Although λ_2 and λ_3 are attracted toward the imaginary axis, they never cross it.

VI. SIMULATION RESULTS

Considering the PV system shown in Fig. 4, different tests have been performed in order to validate the proposed control. All the physical parameters of the system are defined in Table I.

Fig. 12 shows the steady-state current waveforms of the converter, grid, and load (I_C, I_G, and I_L). In the case of a purely resistive load absorbing 1200 W, the block diagram shown in Fig. 8 is modified, taking into account that the active-power reference P_C^* should coincide with the nominal active power and the reactive-power reference $Q_C^* = 0$. The results are shown in Fig. 13. This figure shows the transient response of the active and reactive powers when the active-power reference

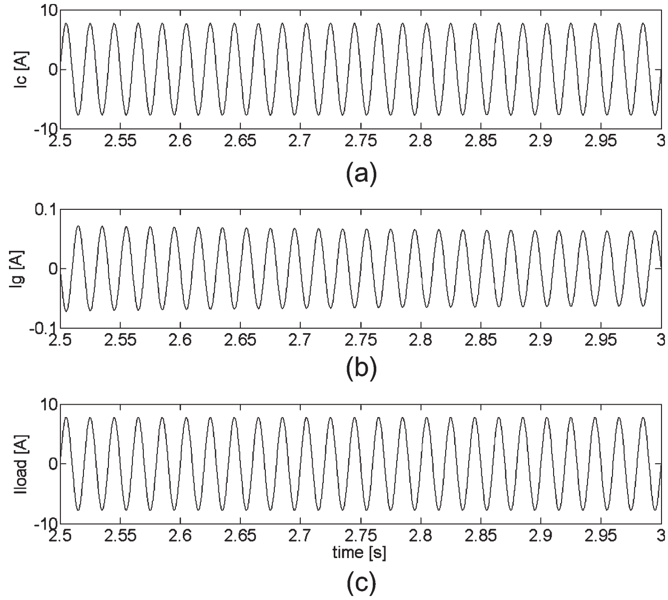

Fig. 12. Steady-state operation during grid normal condition. (a) Inverter current I_C. (b) Grid current I_G. (c) Load current I_L.

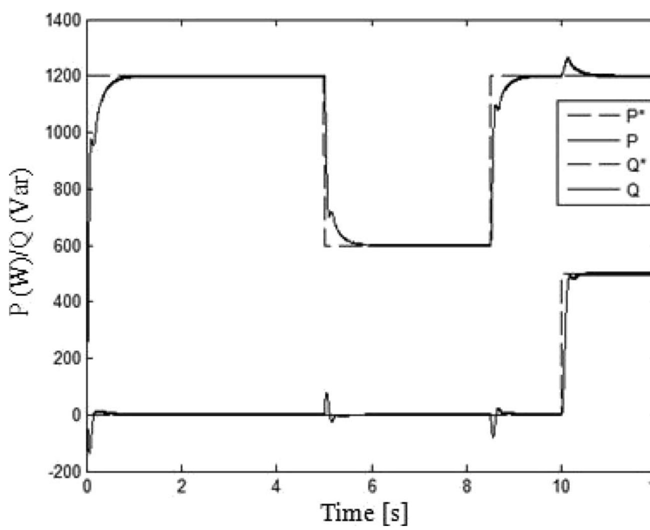

Fig. 13. Active- and reactive-power transient responses and step changes provided by the PV inverter during normal operation.

was changed from 1200 to 600 W at $t = 5$ s and the reactive-power reference from 0 to 500 VAr at $t = 10$ s. The results show the P- and Q-injection decoupling of the proposed control strategy.

The validity of the proposed control has been tested also in the presence of a voltage sag, equals to 0.15 p.u. which occurs at $t = 1.5$ s (see Fig. 14). In this case, the converter provides the reactive power needed to compensate the sag. The current waveforms of the converter, the grid, and the load are shown in Fig. 15. A detail of the grid-voltage and grid-waveforms during the voltage sag is shown in Fig. 16. Notice that the controller endows voltage ride-through capability to the system when voltage sags are presented in the grid.

Similar ride-through capability tests were performed when the active power provided by the inverter (500 W) is lower than the power required by the load. In this situation, the grid

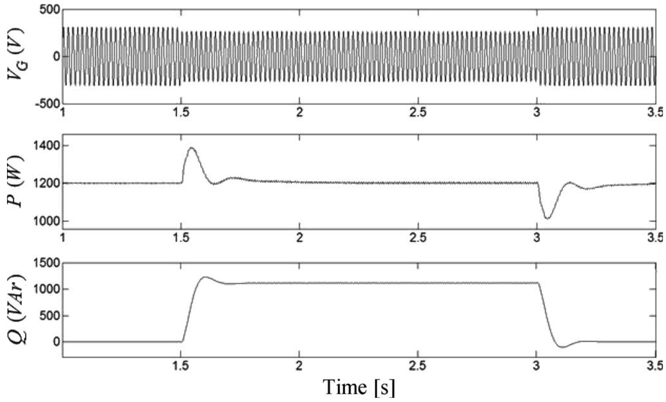

Fig. 14. Active and reactive powers provided by the PV inverter in the presence of a voltage sag of 0.15 p.u.

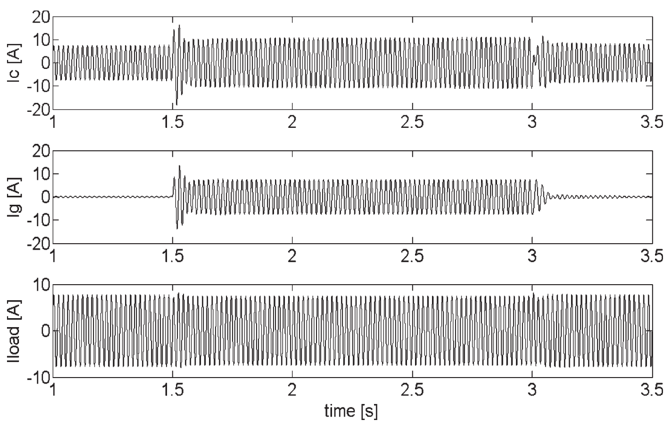

Fig. 15. Current waveforms in case of a voltage sag of 0.15 p.u. (inverter current I_C, grid current I_G, and load current I_L).

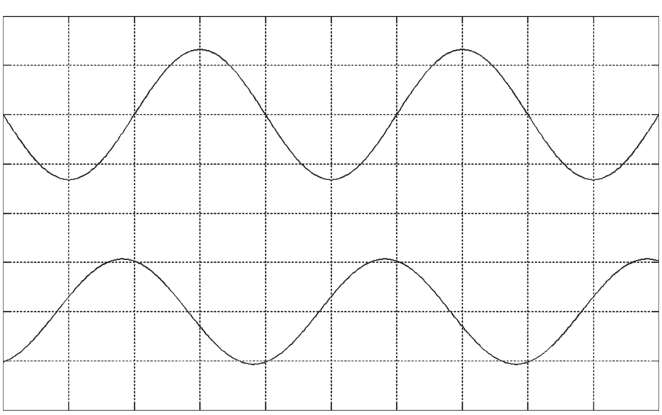

Fig. 16. Detail of the waveforms during the sag. (Upper) Grid voltage [100 V/div]. (Lower) Grid current [10 A/div].

injects the rest of the power to the system (700 W), and the system injects to the grid the necessary reactive power in case of a voltage sag. Fig. 17 shows the active and reactive powers provided by the inverter for a voltage sag, and Fig. 18 shows the corresponding current waveforms. From these results, we can conclude that the system also has ride-through capabilities.

Another test was performed in case of existence of high-value voltage harmonics in the grid, as shown in Fig. 19. Fig. 20 shows the voltage–current waveforms. Note that the system injects harmonic current to the grid in order to maintain the

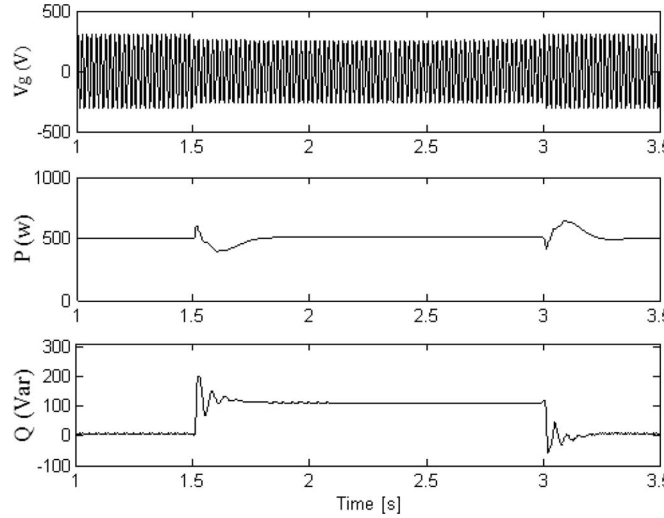

Fig. 17. Active and reactive powers provided by the PV inverter in the presence of a voltage sag of 0.15 p.u. when $P_c^* = 500$ W.

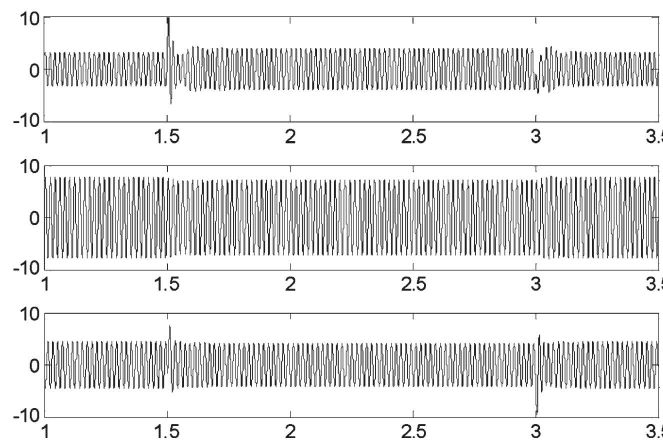

Fig. 18. Current waveforms in case of a voltage sag of 0.15 p.u. (Upper) Inverter current I_C, (middle) load current I_L, and (bottom) grid current I_G, when $P_c^* = 500$ W.

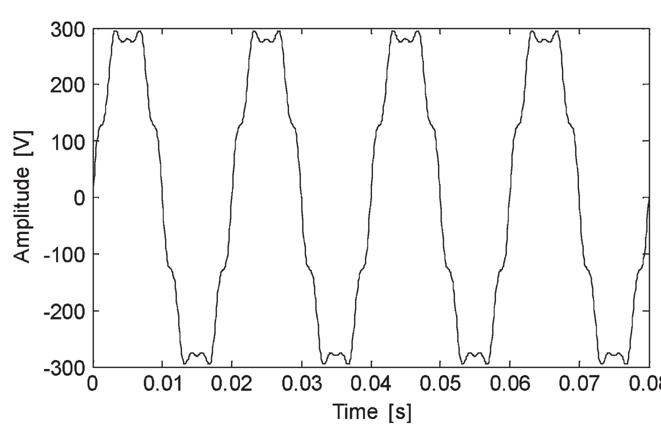

Fig. 19. Grid-voltage waveform in the presence of first, third, fifth, seventh, and ninth voltage harmonics.

quality of the load-voltage waveform. Fig. 20 shows the active- and reactive-power transient responses for changes in the power references, as shown in Fig. 13. In this case, the system also exhibits a good tracking performance.

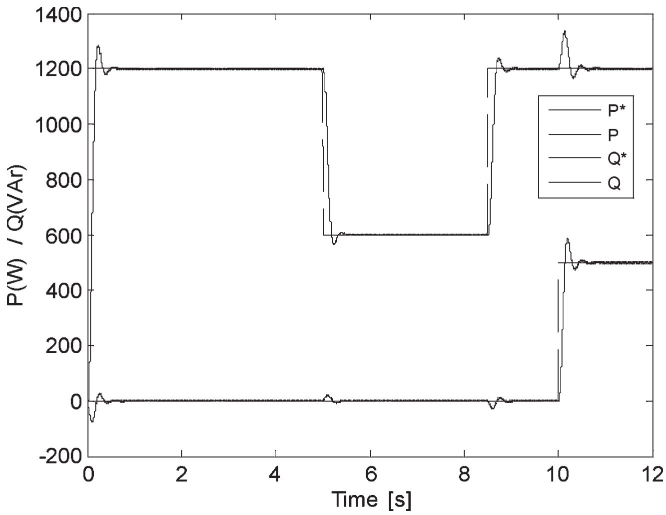

Fig. 20. Active- and reactive-power transient responses and step changes provided by the PV inverter using the distorted grid waveform.

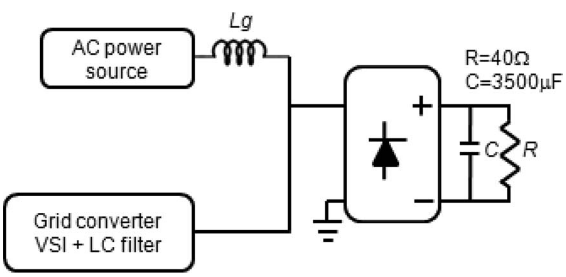

Fig. 21. Single-phase rectifier with RC circuit as nonlinear load.

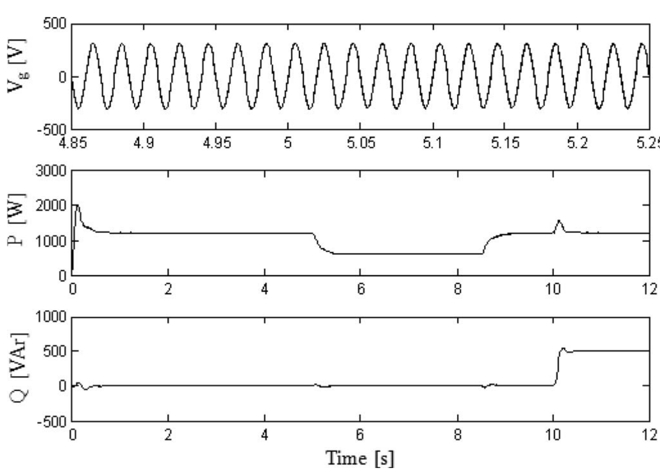

Fig. 22. Inverter output voltage (detail), active- and reactive-power transient responses under a nonlinear load.

Finally, the system was tested by supplying a nonlinear load consisted of a diode rectifier with an RC load, as is shown in Fig. 21. Fig. 22 shows the inverter output voltage and the active and reactive powers provided. This case exhibits the good tracking performance, similar to the case of supplying linear loads (see Fig. 13).

Fig. 23 shows the current waveforms of the inverter, the nonlinear load, and the grid. The system provides shunt active-power capabilities, since the grid current waveform is harmonic-free, and the power factor is near one.

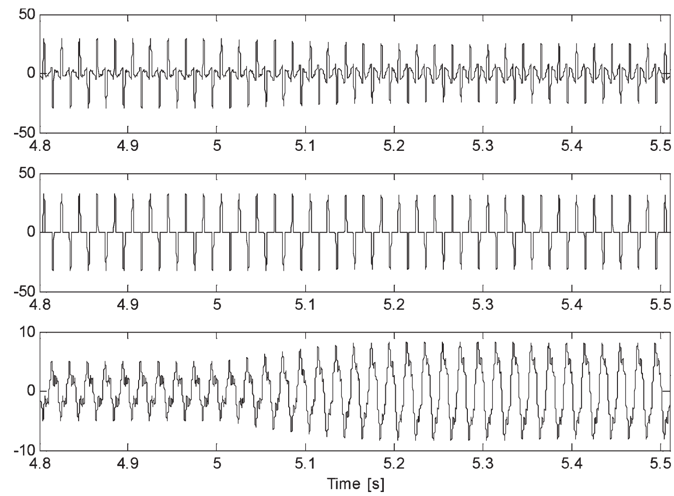

Fig. 23. Current waveforms in case of a nonlinear load and V_g with harmonics. (Upper) Inverter current I_C, (middle) load current I_l, and (bottom) grid current I_G.

According to the obtained results, the system shows high performances like the following: active- and reactive-power tracking, voltage sags ride-through, and voltage- and current-harmonic compensation.

VII. Experimental Results

Experimental results have been carried out in a laboratory setup to test the performance of the PV system with the shunt-connected multifunctional converter. The hardware setup shown in Fig. 24 consists of the following equipment: a Danfoss VLT 5006 7.6-kVA inverter, on which only two legs are used, hence, the apparent power is 2/3 of 7.6 kVA; two series-connected *dc* voltage sources to simulate PV panels string; and Dspace 1104 system. A Pacific ac power source emulates the main grid. It is set in order to provide a voltage sag of 0.15 p.u. The PV multifunctional converter is connected to the grid through an LC filter whose inductance is 1.4 mH, the capacitance is 5 μF in series with a resistance of 1 Ω; besides, an inductance L_G of 15 mH has been added to the grid impedance as explained in the previous sections. The performances of the proposed controllers are in accordance with the simulation results. The experimental results obtained in the same conditions (voltage-sag duration equal to 1.5 s) are shown in Fig. 25.

Figs. 26 and 27 show a detail of the voltage waveforms, the grid voltage, and the injected current during the sag. Notice that PV converter provides voltage support and maintains the load voltage constant by injecting 7 A of pure reactive current into the grid during the voltage sag. These results are in accordance with the simulation tests (see Figs. 14 and 15).

VIII. Conclusion

Future ancillary services in DPGS should contribute to the reinforcement of the distribution grid and to maintain proper quality of supply. In this paper, a single-phase PV system with power quality conditioner functionality is presented. The voltage-controlled PV converter is shunt-connected to the grid, and a droop controller provides the voltage reference. A

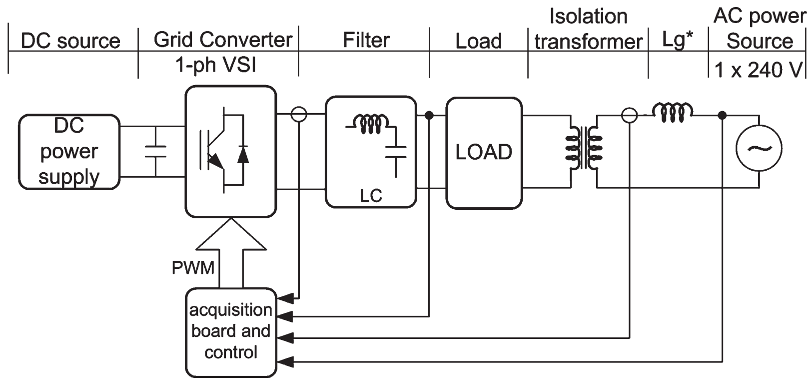

Fig. 24. Laboratory setup.

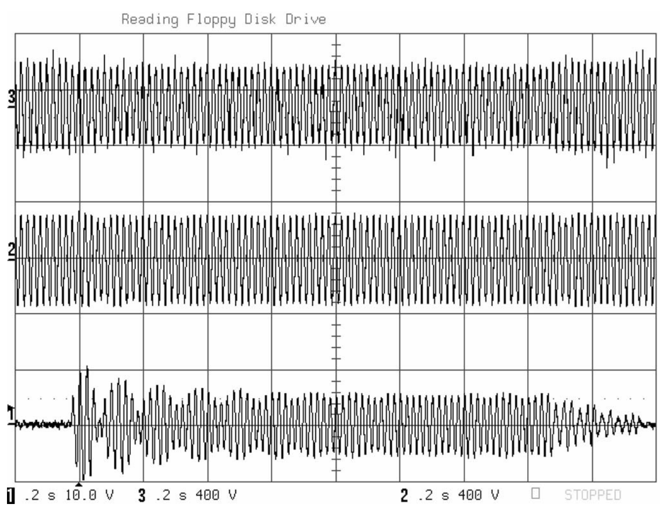

Fig. 25. Experimental results in case of a voltage sag of 0.15 p.u. (voltage-controlled inverter with droop control): (1) grid current [10 V/div], (2) load voltage [400 V/div], and (3) grid voltage [400 V/div].

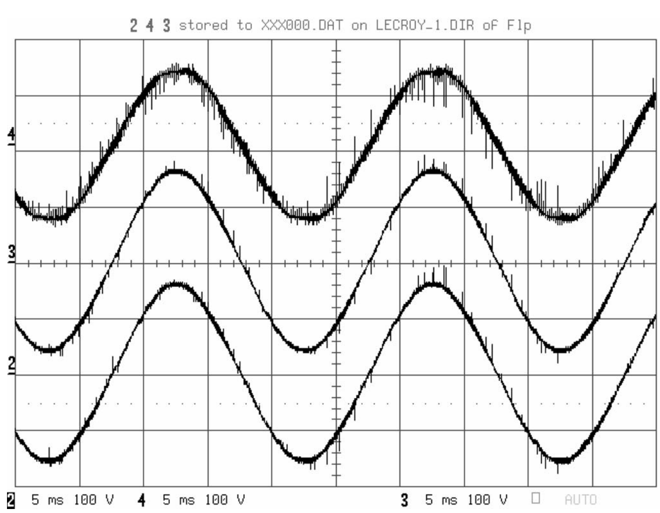

Fig. 26. Voltage waveforms during the sag [100 V/div]. (Channel 4, upper) Grid voltage, (channel 3, middle) capacitor voltage, and (channel 3, lower) load voltage.

repetitive algorithm controls the voltage provided by the PV converter. An inductance has been added on the grid side; hence, it can be considered that the PV system is connected to a mainly inductive grid. It allows the controlling of the grid frequency and the grid-voltage amplitude adjusting active and reactive powers independently.

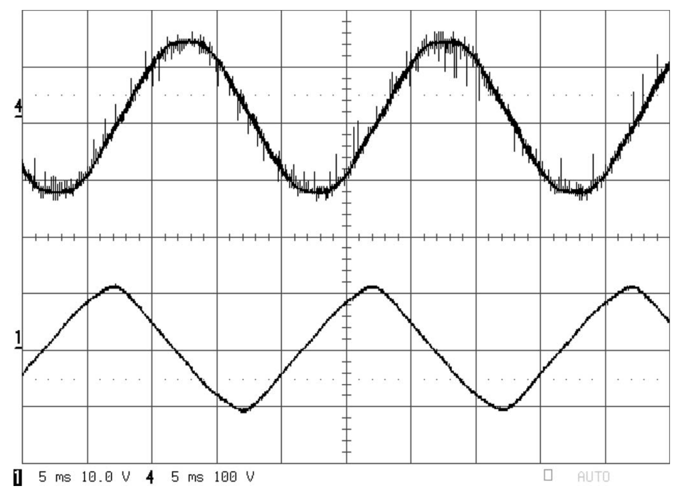

Fig. 27. (Channel 4, upper) Waveforms of the grid voltage [100 V/div] and (channel 1, lower) the grid current [10 A/div] during the sag.

The PV converter provides grid-voltage support at fundamental frequency. In case of a voltage sag, the converter has to provide the active power required by the load and must still inject the reactive power needed to stabilize the load voltage. Hence, the system shows high performances like the following: active- and reactive-power tracking, voltage-sag ride-through, and voltage- and current-harmonic compensation. The experimental results confirm the validity of the proposed solution in the presence of small voltage sags.

REFERENCES

[1] *IEEE Standard for Interconnecting Distributed Resources With Electric Power Systems*, IEEE Std. 1547-2003, 2003.

[2] *IEEE Guide for Monitoring, Information Exchange, and Control of Distributed Resources Interconnected With Electric Power Systems*, IEEE 1547.3-2007, 2007.

[3] F. Blaabjerg, R. Teodorescu, M. Liserre, and A. Timbus, "Overview of control and grid synchronization for distributed power generation systems," *IEEE Trans. Ind. Electron.*, vol. 53, no. 5, pp. 1398–1409, Oct. 2006.

[4] F. Blaabjerg, R. Teodorescu, Z. Chen, and M. Liserre, "Power converters and control of renewable energy systems," in *Proc. Plenary Session Paper ICPE*, Pusan, Korea, Oct. 2004, pp. 2–20.

[5] J. M. Guerrero, J. Matas, L. García de Vicuña, M. Castilla, and J. Miret, "Decentralized control for parallel operation of distributed generation inverters using resistive output impedance," *IEEE Trans. Ind. Electron.*, vol. 54, no. 2, pp. 994–1004, Apr. 2007.

[6] J. M. Guerrero, L. García de Vicuña, M. Castilla, and J. Miret, "Wireless-control strategy for parallel operation of distributed-generation inverters," *IEEE Trans. Ind. Electron.*, vol. 53, no. 5, pp. 1461–1470, Oct. 2006.

[7] J. M. Guerrero, L. García de Vicuña, J. Matas, M. Castilla, and J. Miret, "Output impedance design of parallel-connected UPS inverters with wireless load-sharing control," *IEEE Trans. Ind. Electron.*, vol. 52, no. 4, pp. 1126–1135, Aug. 2005.

[8] J. M. Guerrero, L. García de Vicuña, J. Matas, M. Castilla, and J. Miret, "A wireless controller to enhance dynamic performance of parallel inverters in distributed generation systems," *IEEE Trans. Power Electron.*, vol. 19, no. 5, pp. 1205–1213, Sep. 2004.

[9] R. A. Mastromauro, M. Liserre, and A. Dell'Aquila, "Study of the effects of inductor nonlinear behavior on the performance of current controllers for single-phase PV grid converter," *IEEE Trans. Ind. Electron.*, vol. 55, no. 5, pp. 2043–2052, May 2008.

[10] R. A. Mastromauro, M. Liserre, and A. Dell'Aquila, "Frequency domain analysis of inductor saturation in current controlled grid converters," in *Proc. IEEE IECON*, Nov. 5–8, 2007, pp. 1396–1401.

[11] T. Kawabata, N. Sashida, Y. Yamamoto, K. Ogasawara, and Y. Yamasaki, "Parallel processing inverter system," *IEEE Trans. Power Electron.*, vol. 6, no. 3, pp. 442–450, Jul. 1991.

[12] M. Ashari, C. V. Nayar, and S. Islam, "Steady-state performance of a grid interactive voltage source inverter," in *Proc. IEEE Power Eng. Soc. Summer Meeting*, 2001, pp. 650–655.

[13] C. V. Nayar, M. Ashari, and W. W. K. Keerthipala, "A grid-interactive photovoltaic uninterruptible power supply system using battery storage and a back up diesel generator," *IEEE Trans. Energy Convers.*, vol. 15, no. 3, pp. 348–353, Sep. 2000.

[14] M. Ashari, C. V. Nayar, and W. W. K. Keerthipala, "A single phase parallely connected uninterruptible power supply/demand side management system," *IEEE Trans. Energy Convers.*, vol. 15, no. 1, pp. 97–102, Mar. 2000.

[15] J. M. Guerrero, L. Garcia de Vicuna, and J. Uceda, "Uninterruptible power supply systems provide protection," *IEEE Ind. Electron. Mag.*, vol. 1, no. 1, pp. 28–38, Spring 2007.

[16] H. Tao, J. L. Duarte, and M. A. M. Hendrix, "Line-interactive UPS using a fuel cell as the primary source," *IEEE Trans. Ind. Electron.*, vol. 55, no. 8, pp. 3012–3021, Aug. 2008.

[17] M. Arias, A. Fernandez, D. G. Lamar, M. Rodriguez, and M. M. Hernando, "Simplified voltage-sag filler for line-interactive uninterruptible power supplies," *IEEE Trans. Ind. Electron.*, vol. 55, no. 8, pp. 3005–3011, Aug. 2008.

[18] R. A. Mastromauro, M. Liserre, T. Kerekes, and A. Dell'Aquila, "A single-phase voltage controlled grid connected photovoltaic system with power quality conditioner functionality," *IEEE Trans. Ind. Electron.* to be published.

[19] R. R. Sawant and M. C. Chandorkar, "Methods for multi-functional converter control in three-phase four-wire systems," *IET Power Electron.*, vol. 2, no. 1, pp. 52–66, Jan. 2009.

[20] S.-J. Lee, H. Kim, S.-K. Sul, and F. Blaabjerg, "A novel control algorithm for static series compensator by use of PQR instantaneous power theory," *IEEE Trans. Ind. Electron.*, vol. 19, no. 3, pp. 814–827, May 2004.

[21] C.-C. Shen and C.-N. Lu, "A voltage sag index considering compatibility between equipment and supply," *IEEE Trans. Power Del.*, vol. 22, no. 2, pp. 996–1002, Apr. 2007.

[22] J. Gao, X. H. Zhao, X. Yang, and Z. A. Wang, "The research on avoiding flux imbalance in sinusoidal wave inverter," in *Proc. IEEE IPEMC*, 2000, pp. 1122–1126.

[23] M.-Z. Li and Y. Xing, "Digital voltage regulation with flux balance control for sine wave inverters," in *Proc. IEEE APEC*, 2004, pp. 1709–1713.

Juan C. Vasquez received the B.S. degree in electronics engineering from the Universidad Autonoma de Manizales, Manizales, Colombia, in 2004. He is currently working toward the Ph.D. degree in the Department of Automatic Control Systems and Computer Engineering, Technical University of Catalonia, Barcelona, Spain.

He has been an Assistant Professor with the Universidad Autonoma de Manizales, where he has been teaching courses on digital circuits, servo systems, and flexible manufacturing systems. His research interests include modeling, simulation, and management applied to the distributed generation in microgrids.

R. A. Mastromauro (S'05–M'09) received the M.Sc. and Ph.D. degrees in electrical engineering from the Politecnico di Bari, Bari, Italy, in 2005 and 2009, respectively.

Since 2005, she has been with the Converters, Electrical Machines and Drives Research Team, Department of Electrical and Electronic Engineering, Politecnico di Bari, where she is engaged in teaching courses on power electronics. Her research interests include power converter control for distributed power generation systems based on renewable energies.

Dr. Mastromauro is a member of the IEEE Industrial Electronics Society, the IEEE Power Electronics Society, the IEEE Industrial Application Society, the IEEE Women in Engineering Society, and the Italian Electrotechnical and Electronic Association. She is a reviewer for IEEE conference proceedings and journals.

Josep M. Guerrero (S'01–M'04–SM'08) received the B.S. degree in telecommunications engineering, the M.S. degree in electronics engineering, and the Ph.D. degree in power electronics from the Technical University of Catalonia, Barcelona, Spain, in 1997, 2000, and 2003, respectively.

He is currently an Associate Professor in the Department of Automatic Control Systems and Computer Engineering, Technical University of Catalonia, where he currently teaches courses on digital signal processing, control theory, microprocessors, and renewable energy. Since 2004, he has been responsible for the Renewable Energy Laboratory, Escola Industrial de Barcelona, Barcelona, Spain. His research interests include photovoltaics, wind-energy conversion, uninterruptible power supplies, storage-energy systems, and microgrids.

Dr. Guerrero is the Editor-in-Chief of the *International Journal of Integrated Energy Systems*. He is also an Associate Editor for the IEEE TRANSACTIONS ON INDUSTRIAL ELECTRONICS, the IEEE TRANSACTIONS ON POWER ELECTRONICS, the *International Journal of Power Electronics*, and the *International Journal of Industrial Electronics and Drives*.

Marco Liserre (S'00–M'02–SM'07) received the M.Sc. and Ph.D. degrees in electrical engineering from the Polytechnic of Bari, Bari, Italy, in 1998 and 2002, respectively.

Since January 2004, he has been an Assistant Professor with the Polytechnic of Bari, where he is engaged in teaching courses on power electronics, industrial electronics, and electrical machines. He has been giving lectures in different universities. He has been a Visiting Professor with Aalborg University, Denmark, Alcala de Henares, Spain, and with Christian-Albrechts University of Kiel, Kiel, Germany. He has authored or coauthored more than 127 technical papers, 28 of them published or to be published in international peer-reviewed journals, and three chapters of a book. These works have received more than 800 citations. His current research interests include industrial electronics applications to distributed power generation systems based on renewable energies.

Dr. Liserre is a Senior Member of the IEEE Industrial Electronics Society (IES), the IEEE Power Electronics Society, and the IEEE Industry Applications Society. He was a reviewer for international conferences and journals and has been involved in the IEEE conferences organization in different capacities. Within the IES, he has been responsible for student activities and Region 8 membership activities and has been an Administrative Committee Member and an Editor of the newsletter. He has been giving tutorials for the IEEE Energy Conversion Congress and Exposition (ECCE) 2009, the IEEE Power Electronics Specialists Conference (PESC) 2008, the International Symposium on Industrial Electronics (ISIE) 2008, the European Conference on Power Electronics and Applications (EPE) 2007, the Annual Conference of the IEEE Industrial Electronics Society (IECON) 2006, ISIE 2006, and IECON 2005. He is an Associate Editor of the IEEE TRANSACTIONS ON INDUSTRIAL ELECTRONICS. He is the Founder and has been the Editor-in-Chief of the IEEE INDUSTRIAL ELECTRONICS MAGAZINE in 2007–2009. He is the Founder and the Chairman of the Technical Committee on Renewable Energy Systems of the IES. He has been a Guest Coeditor-in-Chief of the IEEE TRANSACTIONS ON INDUSTRIAL ELECTRONICS for the special section on "Voltage and Current Control of Power Converters." He is also an organizer and a Guest Coeditor-in-Chief of the new special section on "Renewable Energy Systems" of the IEEE TRANSACTIONS ON INDUSTRIAL ELECTRONICS. He will be the Cochairman of ISIE 2010 that will be held in Bari, Italy, on July 4–7, 2010. He was the recipient of the IES 2009 Early Career Award.